Research on gas-liquid-solid three-phase flow model and flow characteristics in deep sea gas hydrate exploitation pipe column

Yuxin Nie [1], Li Mo [1], Xiaoqiang Guo [2]

[1]School of Mechatronic Engineering, Southwest Petroleum University, Chengdu 610500, China

[2]School of Mechanical Engineering, Hebei University of Technology, Tianjin 300401 China

Abstract

In response to the problem of gas-liquid-solid three-phase flow in deep-sea hydrate extraction pipelines, a gas liquid-solid three-phase flow model considering the dynamic decomposition of hydrates is established using continuity equations, momentum equations, and energy equations. flow model considering the dynamic decomposition of hydrates is established using continuity equations, momentum equations, and energy equations. The numerical solution of the theoretical model is achieved using the finite difference method. On this basis, the influence of hydrate abundance, liquid phase displacement, and wellhead back-pressure on the gas-liquid-solid three-dimensional model was investigated. The characteristics in the pipeline was investigated, and it was found that the gas holdup rate will increase with the increase of hydrate abundance. Liquid phase displacement, and wellhead back-pressure, with the influence of hydrate abundance being more sensitive. The liquid holdup rate increases with the increase of hydrate abundance, but decreases first and then increases towards the liquid holdup rate increases with the increase of hydrate abundance, but decreases first and then increases towards the wellhead position with the increase of wellhead back-pressure. The solid phase content decreases with the increase of hydrate abundance. The influence of hydrate abundance on the liquid phase velocity is also relatively small. The solid phase velocity will increase with the increase of hydrate abundance. The research results can provide a theoretical basis for the safety of hydrate mining.

Keywords

Natural gas hydrate; Gas-liquid-solid three-phase flow model; Flow characteristic; Hydrate decomposition.

1. Introduction

The total amount of natural gas hydrate converted to methane gas is about $(1.8 \sim 2.1) \times 10^{16}$ m, the carbon content is more than twice of the total carbon content of all proven fossil fuels, it is a new energy source with the largest reserve that had not yet been exploited [1] and as a kind of low-carbon non-conventional energy source was getting more and more attention, and it was regarded as the most promising energy source of succession in the 21st century, and it was a major need for China's energy security and deep sea strategy to realize the commercial exploitation of natural gas hydrate. The realization of commercial exploitation of natural gas hydrate was a major demand of China's energy security and deep sea strategy.

In the early stage of hydrate decomposition kinetics research, due to the limitation of instrumentation and conditions, most of the researches are at the macroscopic level, such as observing the morphology and microstructure of hydrate decomposition with the help of relevant imaging instruments [2,3] or utilizing the reaction kettle or through the method of injecting heat, depressurization, and chemical agents to study the decomposition kinetics of hydrate [4-6]. With the progress of the times and the updating of the instruments, the research

on hydrate decomposition kinetics has gradually changed from pure water single-component to mixed-component hydrate in porous medium [7], and then based on the thermal decomposition mechanism [8,9], decompression decomposition mechanism [4], and two-step decomposition mechanism [10], scholars have successively established hydrate heat transfer model [9], mass transfer decomposition model [11], and so on. Regarding the research of multiphase flow model, early scholars pioneered the prediction of gas-liquid two-phase flow patterns and obtained the flow pattern distribution diagrams of five flow patterns after a series of corrections and refinements [12,13]. Later scholars established the general two-phase flow mixing model of sand containing [14], which can reveal the pipeline transport situation under different sediment particle sizes and concentrations; the Eulerian-Eulerian two-phase flow model, the population balance model (PBM) and the discrete phase model (DPM) are adopted. The Eulerian-Eulerian two-fluid model, population balance model (PBM) and discrete phase model (DPM) model were used to simulate the three-phase kinetic behavior of gas-liquid-solid, and the results showed that the peak velocity of the liquid phase was reduced due to the presence of the solid phase, and that the gas content rate was almost unchanged with or without the solid phase, and there was no obvious periodical oscillatory plume in the non-Newtonian fluid, and that the solid-liquid interaction had an effect on the flow field, gas distribution and viscosity distribution[15] ; after that some scholars After that, some scholars established a drag model covering two-dimensional and three-dimensional drag interactions, and used the model to improve the radial concentration distribution of gas-solid phases, and found that inside the bubble, the liquid phase follows the motion of the gas phase, while outside the bubble, the liquid phase moves in steps relative to the solid[16, 17] ; In recent years, Zhou proposed a solid-state fluidized mining method for hydrates and established a mathematical model of multiphase flow in the wellbore, and put forward a test method for the inter-particle force of hydrate, and explored the field of the inter-particle force. In recent years, Shouwei Zhou's team proposed the method of hydrate solid state fluidization mining, established a mathematical model of multiphase flow in the wellbore, proposed a test method of hydrate inter-particle force, and explored the influence of field construction parameters on the multiphase non-equilibrium tubular flow, which revealed the flow characteristics of gas-liquid-solid multiphase flow of hydrate [18-20].

Based on this, the current research on hydrates mainly focuses on how to mine and the corresponding geotechnical problems, or for the exploitation of surface hydrates, but lacks a wellbore multiphase flow model and flow characterization for the shallow or deep hydrate mining process containing phase changes. To this end, a gas-liquid-solid three-phase flow model considering the dynamic decomposition of hydrate is established for deep-sea hydrate mining tubular column, and numerical solutions are realized to verify the correctness of the theoretical model with the help of experimental data, on the basis of which, the effects of hydrate abundance, liquid-phase discharge and wellhead backpressure on the content and flow rate of gas-liquid-solid in the tubular column are investigated, and the gas-liquid-solid three-phase flow characteristics are revealed. flow characteristics of gas-liquid-solid.

2. Gas-liquid-solid three-phase flow model in mining columns

2.1. Control equations for gas-liquid-solid three-phase flow

(1) The continuity equation

Take the mixture microelements flowing in the wellbore of length dt ,whose cross-sections are 1-1 and 2-2, respectively, and whose cross-sectional area is A. Take the mixture microelements as the object of study and make the following assumptions about them: (i) the wellbore flow is a continuous medium multiphase flow; (ii) the compression of the liquid phase and the

dissolution of the gas phase are neglected; and (iii) the wellbore flow is a one-dimensional axial flow.

Taking the gas phase as an example, the mass of the gas phase in the control body changes from $\rho_g E_g A dt$ to $\rho_g E_g A dt + \frac{\partial}{\partial z}\left(\rho_g E_g A dz\right) dt$ in dt time, which is obtained from the conservation of mass:

$$\rho_g E_g A dt + q_g = \rho_g E_g A v_g dt + \frac{\partial\left(\rho_g E_g A v_g dt\right)}{\partial z} dz$$
$$+ \frac{\partial\left(\rho_g E_g A v_g dt\right)}{\partial z} dt \tag{1}$$

The gas phase continuity equation in an equal cross-sectional area flow channel is obtained after simplification:

$$\frac{\partial}{\partial t}\left(A \rho_g E_g\right) + \frac{\partial}{\partial z}\left(A \rho_g E_g v_g\right) = q_g \tag{2}$$

Similarly, the liquid-phase continuity equation in an equal cross-sectional area flow channel is obtained:

$$\frac{\partial}{\partial t}\left(A \rho_l E_l\right) + \frac{\partial}{\partial z}\left(A \rho_l E_l v_l\right) = q_l \tag{3}$$

Where ρ_g, ρ_l is the density of gas and liquid phases, kg/m^3; v_g, v_l is the velocity of gas and liquid phases, m/s; E_g, E_l is the holding rate of gas and liquid, dimensionless; q_g is the rate of methane gas produced by the decomposition of natural gas hydrate in the control body, $kg/(s\cdot m)$; q_l is the rate of water produced by the decomposition of natural gas hydrate in the control body, $kg/(s\cdot m)$.
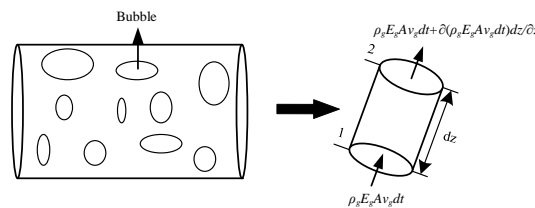

Fig. 1 Controller of gas-phase continuity equation

(2) Momentum equation

According to the conservation of momentum theorem, the rate of change of momentum of an object with respect to time is equal to the sum of the external forces on itself, i.e.:

$$\frac{d}{dt}\left(m\vec{v}\right) = \sum \vec{F} \tag{4}$$

Then the gas-phase momentum equations within the isotropic flow channel control body can be obtained:

$$\frac{\partial}{\partial t}\left(\rho_g E_g v_g\right) + \frac{\partial}{\partial z}\left(p E_g + \rho_g E_g v_g^2\right)$$
$$+ \rho_g E_g g + \frac{\tau_{wg} S_{wg}}{A} + \frac{\tau_i S_i}{A} = 0 \tag{5}$$

Then the gas-liquid-solid mixing momentum equation can be written as:

$$\frac{\partial}{\partial t}\begin{pmatrix} \rho_g E_g v_g \\ + \rho_l E_l v_l + \rho_s E_s v_s \end{pmatrix} + \frac{\partial}{\partial z}\begin{pmatrix} p + \rho_g E_g v_g^2 \\ + \rho_l E_l v_l^2 + \rho_s E_s v_s^2 \end{pmatrix}$$
$$+ \left(\rho_g E_g + \rho_l E_l + \rho_s E_s\right) g + \frac{\lambda \rho_m v_m^2}{2d} = 0 \tag{6}$$

Among them:

$$\frac{\lambda \rho_m v_m^2}{2d} = \frac{\tau_{wg} S_{wg} + \tau_{wl} S_{wl} + \tau_{ws} S_{ws}}{A} \tag{7}$$

Where ρ_g, ρ_l, ρ_s, ρ_m is the density of gas phase, liquid phase, solid phase, mixed phase, kg/m^3; v_g, v_l, v_s, v_m is the flow velocity of gas phase, liquid phase, solid phase, mixed phase, m/s; E_g, E_l, E_s is the gas holding rate, liquid holding rate, solid phase content, dimensionless; p is the pressure of the wellbore, Pa; λ is the coefficient of friction, dimensionless; g is the acceleration of gravity, m/s^2; d is the diameter of the wellbore, m.
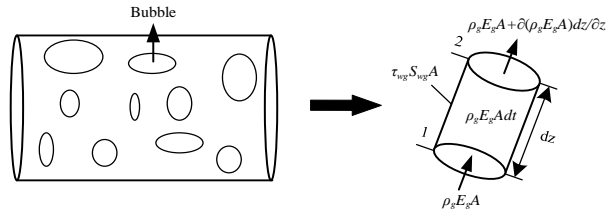

Fig. 2 Gas phase motion control body

(3) Pressure modeling

The pressure in the wellbore consists of gravity pressure drop, friction pressure drop, and acceleration pressure drop, and the pressure model is obtained according to the definition of the three pressure drops as follows:

$$-\frac{dp_a}{dz} = \rho_m g + \frac{2f \rho_m v_m^2}{D_{cn}} + \frac{\rho_m v_m dv_m}{dz} \tag{8}$$

(4) Temperature modeling

As shown in Fig. 3 for the wellbore differential unit heat transfer diagram, take the microelement segment of length dz as the control body, the heat inflow into the control body in dt time q_a, the outflow heat is q_c.
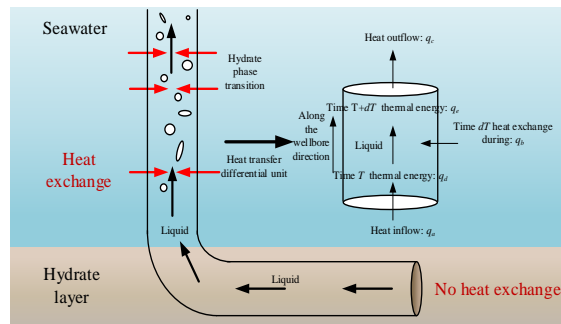

Fig. 3 Heat transfer diagram of wellbore differential unit

then:

$$q_a = \rho_m v_m c_m TS dt + \frac{\partial (\rho_m v_m c_m TS)}{\partial z} dz dt \tag{9}$$

$$q_c = \rho_m v_m c_m TS dt \tag{10}$$

Where T is the fluid temperature, K; v_m is the mixed flow rate, m/s; S is the cross-sectional area, m^2; c_m is the specific heat capacity of the wellbore fluid, J/kg·℃.

dt The heat exchange carried out by the control body during the time is:

$$q_b = q_{wl} + q_f + q_{pt} \tag{11}$$

t moment to control the heat in the body:

$$q_d = \rho_m v_m c_m TS dz \tag{12}$$

$t+dt$ moments to control the heat in the body:

$$q_e = \rho_m v_m c_m TS dz + \frac{\partial (\rho_m v_m c_m TS)}{\partial t} dz dt \tag{13}$$

Heat exchange heat between the fluid inside the microelement body and the outside of the wellbore:

$$q_{wl} = \pi D_{cw} U_{wa} (T_h - T_a) dz dt \tag{14}$$

Among them:

$$U_{wa} = \left[\left(\frac{D_{cw}/D_{cn}}{hr1} \right) + \frac{D_{cw} \ln(D_{cw}/D_{cn})}{2\lambda_c} + \frac{1}{hr2} \right]^{-1} \tag{15}$$

Heat generated by friction between the fluid and the well wall in the micrometabolite:

$$q_f = \frac{2 f v_m^3 \rho_m S}{D_{cn}} dz dt \tag{16}$$

Heat from hydrate phase transitions:

$$q_{pt} = -ZR \cdot \frac{d(\ln p_{ph})}{d(1/T_a)} \cdot n_h S dz dt \tag{17}$$

The temperature equation can be obtained from $q_a - q_c + q_b = q_e - q_d$:

$$\frac{\partial(\rho_m v_m c_m T)}{\partial z} + \pi D_{cw} U_{wa} (T_h - T_a) + \frac{2 f v_m^3 \rho_m S}{D_{cn}}$$

$$-ZR \cdot \frac{d(\ln p_{ph})}{d(1/T_a)} \cdot n_h = \frac{\partial(\rho_m v_m c_m T)}{\partial t} \tag{18}$$

where q_{wl} is the heat exchanged between the fluid in the microcell and the outside of the wellbore, J; q_{fl} is the heat generated by friction between the fluid in the microcell and the well wall, J; q_{pt} is the heat generated by the phase change of the hydrate in the microcell, J. D_{cw}、D_{cn} are the outer and inner diameters of the tubular column, m; T_h、T_a are the temperature of seawater and the wellbore, respectively, K; $hr1$ is the coefficient of forced convective heat transfer on the inner surface of the mining tubular column; $hr2$ is the coefficient of natural convective heat transfer on the outer surface of the mining tubular column; f is the flow resistance coefficient; c_m is the specific heat capacity of wellbore fluid; J/kg·℃; p_a is the wellbore pressure, Pa; Z is the natural gas compression factor; R is the universal gas constant, 8.314 J·mol^{-1}·K^{-1}; p_{ph} is the phase equilibrium pressure at the temperature of the wellbore, MPa; and $\frac{dn_h}{dt}$ is the total hydrate decomposition rate per unit length, mol/s.

2.2. Three-phase flow pattern discrimination

Fluid flow along the wellbore process with different locations will appear different flow patterns, and different flow patterns need to choose its appropriate model. According to the range limited by various flow patterns in the flow pattern diagram, the discriminant relationship between various flow patterns of two-phase flow can be obtained [13]:

(1) Vesicular flow

$$\begin{cases} v_{sg} < 0.429 v_{sl} + 0.357 v_{0\infty} \\ d > 19.01 \sqrt{\dfrac{\sigma}{g(\rho_l - \rho_g)}} \end{cases} \tag{19}$$

(2) Dispersing bubble flow

$$\begin{cases} v_{sg} < 1.08 v_{sl} \\ 2 \left[\dfrac{0.4\sigma}{g(\rho_l - \rho_g)} \right]^{-0.5} \left(\dfrac{\rho_l}{\sigma} \right)^{0.6} \left(\dfrac{2f}{d} \right)^{0.4} v_m^{1.2} > 0.725 + 4.15 \left(\dfrac{v_{sg}}{v_m} \right) \end{cases} \tag{20}$$

(3) Segmental plug flow

$$\begin{cases} v_{sg} \geq 0.429 v_{sl} + 0.357 v_{0\infty} \\ v_{sg} \geq 1.08 v_{sl} \end{cases} \tag{21}$$

(4) Churning flow

$$\begin{cases} 0.058 \left\{ 2 \left[\dfrac{0.4\sigma}{g(\rho_l - \rho_g)} \right]^{-0.5} \left(\dfrac{\rho_l}{\sigma} \right)^{0.6} \left(\dfrac{2 f v_m^3}{d} \right) - 0.725 \right\}^2 \geq 0.52 \\ v_{sg} < 3.1 \left[\dfrac{g\sigma(\rho_l - \rho_g)}{\rho_g^2} \right]^{0.25} \end{cases} \tag{22}$$

(5) Circum-fog flow

$$v_{sg} \geq 3.1 \left[\frac{g\sigma(\rho_l - \rho_g)}{\rho_g^2} \right]^{0.25} \tag{23}$$

Where: v_{sg} is the apparent gas phase flow rate, m/s; v_{sl} is the apparent liquid phase flow rate, m/s; v_m is the mixed flow rate, m/s; A is the area of the flow channel, m² ; d is the diameter of the pipe, m; g is the acceleration of gravity, m/s² ; f is the coefficient of friction, no cause and effect; σ is the interfacial tension between the gas and liquid phases, N/m; ρ_g , ρ_l is the density of the gas and liquid phases, kg/m³ ; $v_{0\infty}$ is the rising velocity of a single bubble in the infinite medium, m/s.

2.3. Solving the model

The equations are discretized using the finite difference method, which is calculated from the bottom of the well to the top of the well in the following difference format:

Continuity equation discretization, gas phase:

$$\frac{1}{2\Delta t_i} \left[\left(A\rho_g E_g \right)_{i+1}^{n+1} - \left(A\rho_g E_g \right)_{i+1}^{n} + \left(A\rho_g E_g \right)_{i}^{n+1} - \left(A\rho_g E_g \right)_{i}^{n} \right]$$
$$+ \frac{1}{\Delta z_i} \left[\left(A\rho_g E_g v_g \right)_{i+1}^{n+1} - \left(A\rho_g E_g v_g \right)_{i}^{n+1} \right] = \frac{1}{2} \left[\left(q_g \right)_{i+1}^{n+1} + \left(q_g \right)_{i}^{n+1} \right] \tag{24}$$

Liquid phase:

$$\frac{1}{2\Delta t_i} \left[\left(A\rho_l E_l \right)_{i+1}^{n+1} - \left(A\rho_l E_l \right)_{i+1}^{n} + \left(A\rho_l E_l \right)_{i}^{n+1} - \left(A\rho_l E_l \right)_{i}^{n} \right]$$
$$+ \frac{1}{\Delta z_i} \left[\left(A\rho_l E_l v_l \right)_{i+1}^{n+1} - \left(A\rho_l E_l v_l \right)_{i}^{n+1} \right] = \frac{1}{2} \left[\left(q_l \right)_{i+1}^{n+1} + \left(q_l \right)_{i}^{n+1} \right] \tag{25}$$

Hydrate particles:

$$\frac{1}{2\Delta t_i} \left[\left(A\rho_s E_s \right)_{i+1}^{n+1} - \left(A\rho_s E_s \right)_{i+1}^{n} + \left(A\rho_s E_s \right)_{i}^{n+1} - \left(A\rho_s E_s \right)_{i}^{n} \right]$$
$$+ \frac{1}{\Delta z_i} \left[\left(A\rho_s E_s v_s \right)_{i+1}^{n+1} - \left(A\rho_s E_s v_s \right)_{i}^{n+1} \right] = \frac{1}{2} \left[\left(q_s \right)_{i+1}^{n+1} + \left(q_s \right)_{i}^{n+1} \right] \tag{26}$$

Momentum equation discretization:

$$\frac{1}{2\Delta t_i} \left[\left(\rho_g E_g v_g \right)_{i+1}^{n+1} - \left(\rho_g E_g v_g \right)_{i+1}^{n} + \left(\rho_g E_g v_g \right)_{i}^{n+1} - \left(\rho_g E_g v_g \right)_{i}^{n} \right]$$
$$+ \frac{1}{\Delta z_i} \left[\left(pE_g + \rho_g E_g v_g^2 \right)_{i+1}^{n+1} - \left(pE_g + \rho_g E_g v_g^2 \right)_{i}^{n+1} \right]$$
$$= -\frac{1}{2} \left[\left(\rho_g E_g g + \frac{\tau_{wg} S_{wg}}{A} \right)_{i+1}^{n+1} + \left(\rho_g E_g g + \frac{\tau_{wg} S_{wg}}{A} \right)_{i}^{n+1} \right] \tag{27}$$

$$\frac{1}{2\Delta t_i}\left[\left(\rho_l E_l v_l\right)_{i+1}^{n+1}-\left(\rho_l E_l v_l\right)_{i+1}^{n}+\left(\rho_l E_l v_l\right)_{i}^{n+1}-\left(\rho_l E_l v_l\right)_{i}^{n}\right]$$

$$+\frac{1}{\Delta z_i}\left[\left(pE_l+\rho_l E_l v_l^2\right)_{i+1}^{n+1}-\left(pE_l+\rho_l E_l v_l^2\right)_{i}^{n+1}\right] \tag{28}$$

$$=-\frac{1}{2}\left[\left(\rho_l E_l g+\frac{\tau_{wl}S_{wl}}{A}\right)_{i+1}^{n+1}+\left(\rho_l E_l g+\frac{\tau_{wl}S_{wl}}{A}\right)_{i}^{n+1}\right]$$

$$\frac{1}{2\Delta t_i}\left[\left(\rho_s E_s v_s\right)_{i+1}^{n+1}-\left(\rho_s E_s v_s\right)_{i+1}^{n}+\left(\rho_s E_s v_s\right)_{i}^{n+1}-\left(\rho_s E_s v_s\right)_{i}^{n}\right]$$

$$+\frac{1}{\Delta z_i}\left[\left(pE_s+\rho_s E_s v_s^2\right)_{i+1}^{n+1}-\left(pE_s+\rho_s E_s v_s^2\right)_{i}^{n+1}\right] \tag{29}$$

$$=-\frac{1}{2}\left[\left(\rho_s E_s g+\frac{\tau_{ws}S_{ws}}{A}\right)_{i+1}^{n+1}+\left(\rho_s E_s g+\frac{\tau_{ws}S_{ws}}{A}\right)_{i}^{n+1}\right]$$

$$\frac{1}{2\Delta t_i}\left[\begin{array}{l}\left(\rho_m v_m c_m T\right)_{i+1}^{n+1}-\left(\rho_m v_m c_m T\right)_{i+1}^{n}\\+\left(\rho_m v_m c_m T\right)_{i}^{n+1}-\left(\rho_m v_m c_m T\right)_{i}^{n}\end{array}\right]$$

$$+\frac{1}{\Delta z_i}\left[\left(\rho_m v_m c_m T\right)_{i+1}^{n+1}-\left(\rho_m v_m c_m T\right)_{i}^{n+1}\right]$$

$$=-\frac{1}{2}\left[\begin{array}{l}\left(\begin{array}{l}\pi D_{cw}U_{wa}\left(T_h-T_a\right)+\dfrac{2fv_m^3\rho_m S}{D_{cn}}\\[2mm]-\left(-ZR\right)\cdot\dfrac{d\left(\ln p_{ph}\right)}{d\left(1/T_a\right)}\cdot n_h\end{array}\right)_{i+1}^{n+1}\\[10mm]+\left(\begin{array}{l}\pi D_{cw}U_{wa}\left(T_h-T_a\right)+\dfrac{2fv_m^3\rho_m S}{D_{cn}}\\[2mm]-\left(-ZR\right)\cdot\dfrac{d\left(\ln p_{ph}\right)}{d\left(1/T_a\right)}\cdot n_h\end{array}\right)_{i}^{n+1}\end{array}\right] \tag{30}$$

The specific numerical solution process is shown in Fig. 4:

3. Gas-liquid-solid three-phase flow characteristics

The gas-liquid-solid three-phase flow characteristics of deep-sea natural gas hydrate mining tubular column are affected by hydrate abundance, so the established hydrate gas-liquid-solid three-phase flow model was used to investigate the influence law of the three on the gas-liquid-solid three-phase flow characteristics, to reveal the hydrate flow characteristics, and put forward corresponding parameter configuration scheme. The basic parameters are as follows: diameter of mining pipe column: 0.508 m, density of drilling fluid is seawater density i.e. 1030 kg/m3, hydrate particle size is 5 mm, water depth is 1000 m, seawater density is 1030 kg/m3, well depth is 1400 m, depth of inclined section is 830 m~1100 m, and depth of horizontal section is 1100 m~1400 m, and the temperature of the sea surface is 293 K. The parameters are as follows. By setting the wellhead backpressure 0.1 MPa, liquid phase displacement 30 L/s, hydrate abundance 60%, 70%, 80%, respectively, the velocity of each phase and the content of each item in the wellbore under different hydrate abundance are calculated, as shown in Figs. 5 and 6, from which it can be seen that, in the horizontal section from 1400 to 1100 m, the solid-phase velocity, liquid-phase velocity, liquid-holding rate and solid-phase content are unchanged, and the gas-holding rate and gas-phase content are zero, since the hydrate is not decomposed. hydrate is not decomposed, so the gas-holding rate and gas-phase velocity are

zero; in the vertical section from 1100~840 m diagonal section to the hydrate decomposition position: the higher the hydrate abundance is, the lower the density of hydrate is, and the easier it is to be carried, so the solid-phase content decreases with the increase of hydrate abundance, while the liquid-holding rate increases. At the same time, due to the hydrate is about to decompose, the gas phase velocity will have a certain degree of increase, and because with the increase of hydrate abundance, the solid phase density decreases, then the solid phase transportation speed will increase, i.e., the liquid phase velocity will have a certain degree of increase. As the hydrate has not been decomposed, the gas phase velocity and gas holding rate are still zero; after the hydrate decomposition is complete: with the increase of hydrate abundance, the total amount of gas produced by decomposition will also increase, then the gas holding rate increases, and the gas expansion will lead to the increase of gas phase velocity as well as the liquid phase velocity, and the decomposition of the remaining solid phase will be reduced, i.e., the solid-phase content decreases.
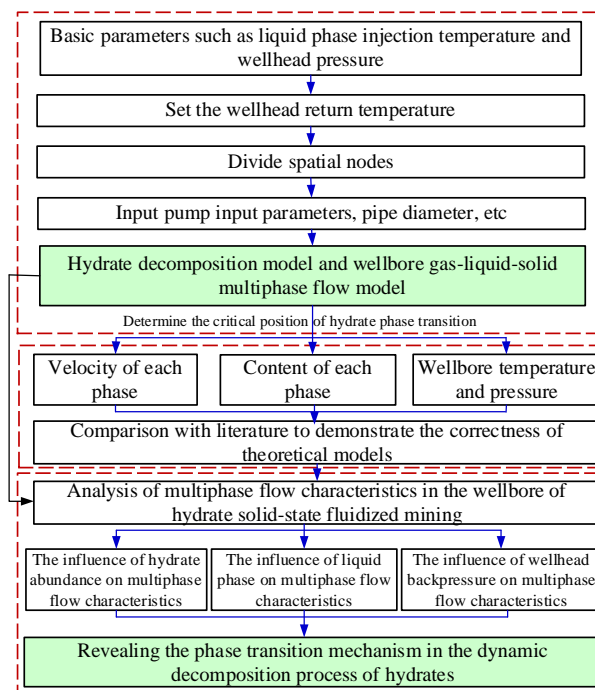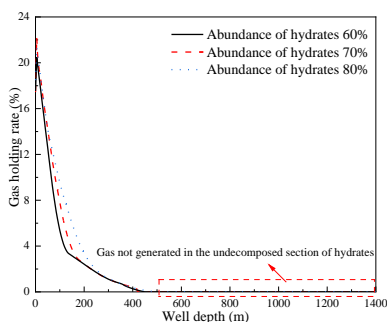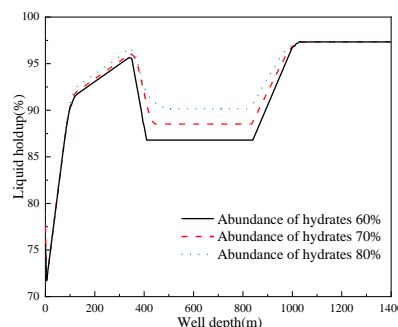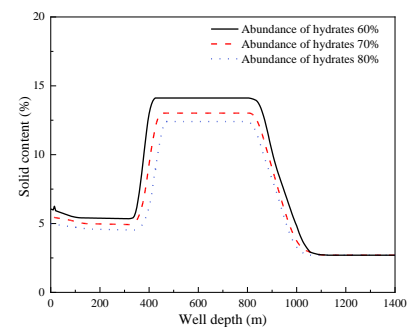

Fig. 4 Flowchart of numerical solution

(a) Distribution of gas phase content

(b) Liquid phase content distribution

(c) Distribution of solid phase content

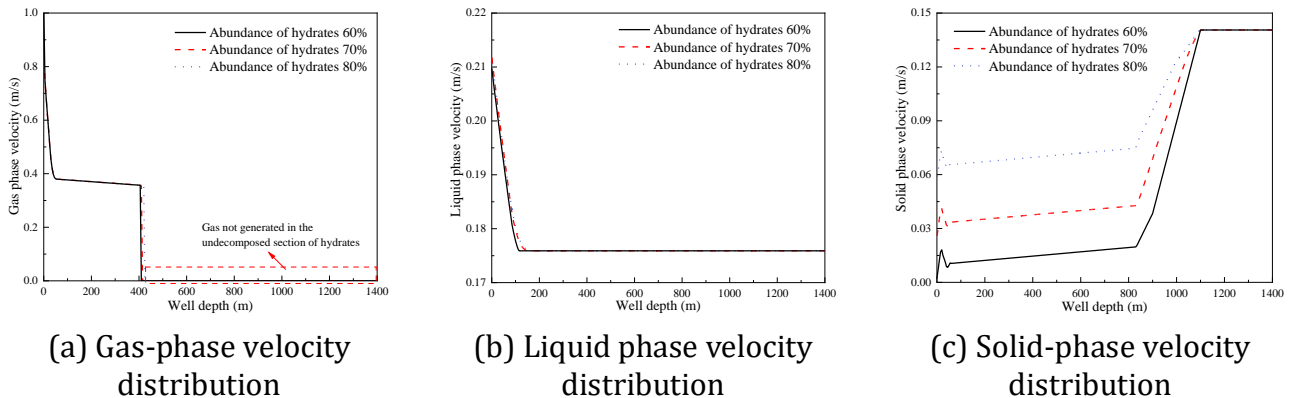Fig. 5 Distribution of various contents with well depth for different hydrate abundances

| (a) Gas-phase velocity distribution | (b) Liquid phase velocity distribution | (c) Solid-phase velocity distribution |

Fig. 6 Distribution of each rate with well depth for different hydrate abundances

4. Conclusion

The established hydrate gas-liquid-solid three-phase flow model is used to investigate the effects of hydrate abundance, liquid phase displacement and wellhead back pressure on the gas-liquid-solid three-phase flow characteristics, and to reveal the hydrate flow characteristics, and it is found that: the gas-holding rate increases with the increase of hydrate abundance, liquid phase displacement, and wellhead back pressure, in which the effect of hydrate abundance is more sensitive, the main reason for this is that the higher the abundance of hydrate. The main reason is that the higher the hydrate abundance, the lower the hydrate density and the easier it is to be carried.

Liquid-holding rate will increase with the increase of hydrate abundance; solid-phase content will decrease with the increase of hydrate abundance. The reason is that the larger the wellhead backpressure is, the smaller the gas expansion is, therefore, with the increase of wellhead backpressure, the gas-holding rate and liquid-holding rate will also decrease, but the solid-phase content increases, after that, with the more serious decomposition of hydrate, the gas phase is more, the gas-holding rate will continue to increase. The reason is that the more wellhead backpressure, the less gas expansion, so with the increase of wellhead backpressure, the gas holding rate and liquid holding rate will decrease, but the solid phase content will increase, after that, with the hydrate decomposition is more serious, the gas phase is more, the gas holding rate continues to increase, in the case of wellhead backpressure increase, the multi-phase flow will be compressed more seriously, the mixing density will be reduced, so the rock-carrying ability is strong, therefore, the solid phase content has a mutation to reduce the rate of the liquid holding rate is also a mutation to increase instead.

References

[1]   WU Xishun, HUANG Wenbin, LIU Wenchao, et al. Evaluation of global gas hydrate resource potential and progress of exploration and test mining[J]. Frontiers of Marine Geology, 2017, 33(7):63-78.

[2]   ARVIND G, GEORGE J M, TIMOTHY J K, et al. Modeling pure methane hydrate dissociation using a numerical simulator from a novel combination of x-ray computed tomography and macroscopic data[J]. Energy & Fuels. 2010, 23(12): 5958-5965.

[3]   SHI Bohui, WANG Ying, LU Xiaofang, et al. Progress of hydrate decomposition research in flow system[J]. Oil and Gas Storage and Transportation, 2014, (7): 685-691.

[4]   KIM H C, BISHNOI P R, HEIDEMANN R A, et al. Kinetics of methane hydrate decomposition[J]. Chemical Engineering Science. 1987, 42(7): 1645-1653.

[5]   CLARKE M, BISHNOI P R. Determination of the intrinsic rate of ethane gas hydrate decomposition[J]. Chemical Engineering Science. 2000, 55(21): 4869-4883.

[6]   WINDMEIER C, OELLRICH L R. Experimental study of methane hydrate decomposition kinetics[J]. Chemie Ingenieur Technik. 2015, 87(7): 910-921.

[7]   YU Guigang, OU Wenjia, WU Xiang, et al. Progress on the decomposition kinetics of natural gas hydrates[J]. Geoscience Bulletin, 2023, 42(3): 175-188.

[8]   KAMATH V A, HOLDER G D, ANGERT P F. 3 Phase interfacial heat-transfer during the dissociation of propane hydrates[J]. Chemical Engineering Science. 1984, 39(10): 1435-1442

[9]   KAMATH V A, HOLDER G D, Dissociation heat transfer characteristics of methane hydrates[J]. AIChE Journal. 1987, 33(2): 347-350

[10] HANDA Y P. A calorimetric study of naturally occurring gas hydrates[J]. Industrial & Engineering Chemistry Research. 1988, 27(5): 872-874

[11] TAKEYA S, EBINUMA T, UCHIDA T, et al. Self-preservation effect and dissociation rates of CH4 hydrate[J]. Journal of Crystal Growth. 2002, 237-239: 379-382.

[12] LOPES J C B, DUKLER A E. Droplet entrainment in vertical annular flow and its contribution to momentum transfer[J]. AIChE Journal, 1986, 32(9): 1500-1515

[13] HASAN A R. Predicting multiphase flow behavior in a deviated well[J]. SPE Production Engineering, 1988, 3(4): 474-482

[14] WANG Le, CAO Zhourong, CAI Hulin, et al. Numerical simulation of gas-liquid-solid three phase in bubble column[C]. Journal of Physics: Conference Series, 2021, 1739(1): 012041

[15] LI Jiaxing, CHEN Xin. A general two-phase mixture model for sediment-laden flow in open channel[J]. Journal of Hydrodynamics, 2022, (2): 286-298

[16] YU Yang, SUO Tongchuan, TAN Wei, et al. Numerical simulation of gas-liquid-solid three-phase flow with the construction of theoretical continuous elements.[J]. Chemical Engineering Science, 2020, 220

[17] WASHINO K, CHAN E L, KAJI T, et al. On large scale CFD-DEM simulation for gas-liquid-solid three-phase flows[J] . . Particuology, 2020, 59: 2-15

[18] WEI Na, SUN Wantong, Meng Yingfeng, et al. Change mechanism of transient gas-liquid two-phase flow in wellbore during marine natural gas hydrate reservoir drilling[J]. Thermal Science, 2019,23(4): 2179-2187.

[19] WEI Na, ZHAO Jinzhou, SUN Wantong, et al. Multiphase non-equilibrium pipe flow characteristics of solid-state fluidized extraction of marine gas hydrate reservoirs[J]. Natural Gas Industry, 2018, 38(10): 90-99.

[20] WEI Na, SUN Wangtong, MENG Yingfeng, et al. Sensitivity analysis of multiphase flow in annulus during drilling of marine natural gas hydrate reservoirs [J]. Journal of Natural Gas Science & Engineering, 2016, 36: 692-707.